

Optimization of Plasma Initiation Scenarios in JT-60SA

Makoto MATSUKAWA¹, Tsunehisa TERAKADO¹, Kunihiro YAMAUCHI¹, Katsuhiro SHIMADA¹, Philippe CARA², Elena GAIO³, Luca NOVELLO³ Alberto FERRO³, Roberto COLETTI⁴, Maurizio Santinelli⁴ and Alberto COLETTI⁵

¹*Japan Atomic Energy Agency, 801-1 Mukoyama, Naka, Ibaraki 311-0119, Japan*

²*CEA, IRFM, F-13108 Saint-Paul-lez-Durance, France*

³*Consorzio RFX - EURATOM ENEA Association, C.so Stati Uniti 4, 35127 Padova, Italy*

⁴*ENEA, Frascati, Italy*

⁵*Fusion for Energy, Garching, Germany*

(Received: 30 October 2009 / Accepted: 24 February 2010)

Stable plasma initiation is very important in nuclear fusion devices especially in superconducting tokamaks, because available electric field at breakdown will be limited to the range of 0.3~0.5 V/m for suppressing large AC losses in the superconducting magnet. However, induced current in passive structures such as vacuum vessel and stabilizing plate will increase to the comparable level of plasma current of several hundred kA even in the case of breakdown assisted by Electron Cyclotron Heating (ECH), and it will enhance the strength of error field. Therefore, optimization of the voltage waveforms of poloidal field coil is necessary to realize the stable plasma initiation. In this paper, magnetic field control method for the stable plasma initiation and cost effectively designed magnet power supply system in JT-60SA are presented.

Keywords: JT-60SA, Breakdown, Plasma initiation, Error field, Electric field, Power supply

1. Introduction

Stable plasma initiation in tokamak devices will be obtained by a combination of good wall conditioning with following precise magnetic field control and gas puffing. This condition was studied experimentally at worldwide tokamaks [1-2], and the obtained result is now recognized as a basis of the design condition in ITER [3]. In principle, the same plasma initiation condition of ITER can be applied to JT-60SA, because JT-60SA is a sufficiently large superconducting tokamak [4]. It must be noted that the maximum applicable breakdown electric field was raised up to 0.5 V/m in JT-60SA, taking into account the relatively lower toroidal magnetic field strength of 2.3 T. The ECH assist at breakdown (<3MW) is planned as well as ITER [5].

For accurate analysis, the passive structure of tokamak must be modeled with 3D elements as precisely as possible, but it is not so easy because each section has different port geometries for plasma heating and diagnostic devices. Then, we used 2D model for the simplicity, and to keep the flexibility in analysis. As a result, the vacuum vessel and stabilizing plate were modeled by about 100 passive poloidal field coils. For deriving the applied voltage waveforms, the following conditions are taken into account: (1) Breakdown electric field 0.5 V/m, (2) Breakdown area larger than 1 m², (3) Maximum experienced magnetic field strength of 8.9 T at the central solenoid (CS).

In this paper, short description of JT-60SA magnets

and some static analysis results in pre-magnetization phase are mentioned in section 2. The passive coil model is presented in section 3. Optimization procedure of plasma initiation is described in section 4, and switching network unit (SNU) of power supply system is shortly given in section 5. The obtained typical plasma initiation scenario is described in section 6, and a discussion is made in section 7. Summary is presented in section 8.

2. Static Analysis of the Error Field

In the superconducting tokamaks, the maximum experienced magnetic field strength at conductor must be taken into account as one of their operational limit as well as the maximum current. The static analysis of the error field at pre-magnetization phase was carried out as follows:

Step.1: Defining the reference point of supplied flux evaluation and plasma breakdown area (null field) in the vacuum vessel as shown in Fig. 1.

Step 2: Defining the evaluating points of field strength (B_{max}) at the conductor surface of poloidal field coils.

Step 3: Obtaining the optimized current distribution at pre-magnetization phase with constrains of the maximum experienced magnetic field strength as shown in table 1.

Figure 1 shows the geometric relationship of above mentioned procedure in the JT-60SA. In this case, the circular area of null field was specified, and the maximum field strength was evaluated at the conductor surface with every 2 cm pitch.

Table 1. Poloidal field coil data of JT-60SA.

Coil	R (m)	Z (m)	Turn	dR (m)	dZ (m)	B _{max} (T)
CS1	0.822	2.407	554	0.327	1.574	8.9
CS2	0.822	0.802	554	0.327	1.574	8.9
CS3	0.822	-0.802	554	0.327	1.574	8.9
CS4	0.822	-2.407	554	0.327	1.574	8.9
EF1	5.801	1.179	142	0.329	0.334	4.8
EF2	4.607	3.171	154	0.357	0.334	4.8
EF3	1.913	4.025	247	0.543	0.428	6.2
EF4	1.913	-4.117	353	0.543	0.611	6.2
EF5	3.902	-3.722	152	0.302	0.390	4.8
EF6	5.039	-2.772	180	0.357	0.390	4.8

Notice: Coil current rating is 20 kA for all PF coils.

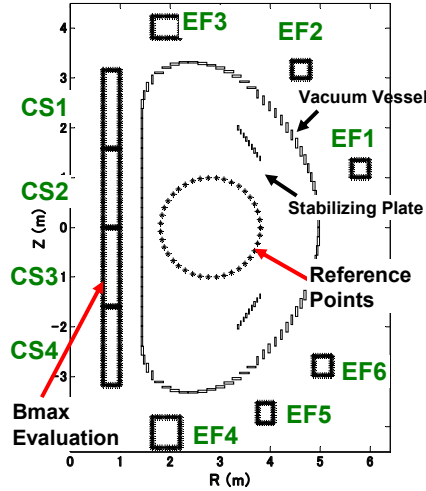


Fig. 1. An example of Reference Points and B_{max} Evaluation Points with passive coil model of vacuum vessel and stabilizing plate.

Figure 2 shows the various results of null field regimes (breakdown area), and the PF coil current is summarized in table 2. It is clear that 10 PF coil system can produce a variety of null field. It must be noted that the amount of total supplied flux will be changed according to the shape of null field. Figure 3 shows the PF coil current distribution for the created pre-magnetization database. Larger current change of the outer poloidal field coils (EF1-2, EF5-6) has been observed, because they have large contribution on the error field compensation. In other words, the rationalization of the Ampere-Turn of these coils shall be possible. As a conclusion, we have decided to limit the coil current of EF1-2 and EF5-6 to be less than ± 4 kA in the pre-magnetization phase.

3. Passive Coil Model

Figure 4 shows the 2D model used in this work. Here, the vacuum vessel and stabilizing plate are modeled by finite number of resistive poloidal field coil which has

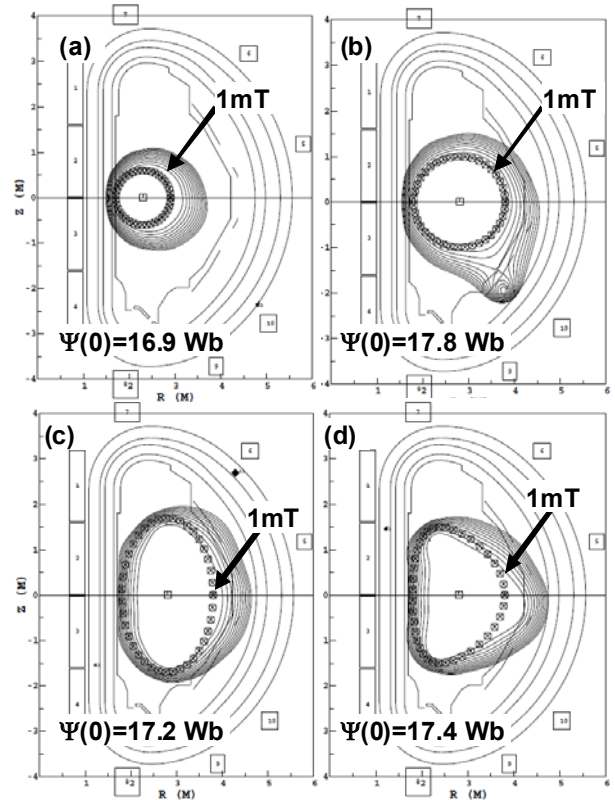


Fig. 2. Null field regimes for various coil current sets.

Table 2. PF coil currents of static analysis results (kA).

Coil	Case (a)	Case (b)	Case (c)	Case (d)
CS1	17.56	19.58	20.00	20.00
CS2	18.20	19.07	18.31	18.52
CS3	18.15	19.02	18.39	18.59
CS4	18.09	20.00	19.64	19.63
EF1	-2.777	1.367	1.004	1.074
EF2	-3.035	-0.1112	0.7695	0.4848
EF3	20.00	16.17	13.40	14.22
EF4	13.45	11.38	11.48	12.58
EF5	-1.777	-0.8427	-2.256	-3.498
EF6	0.549	1.298	1.892	2.261

equivalent electric resistance. For the stability of numerical analysis and shortening the calculation time, the number of passive coil model was set to around 100 based on our experiences. The electric resistance of vacuum vessel in the toroidal direction was estimated to be $16.5 \mu\Omega$ for the model of Fig.4 (a) which does not have port hole. This resistance value is approximately one tenth of present JT-60U.

When the maximum breakdown electric field of 0.5 V/m was applied, the induced current in the vacuum vessel may exceed 500 kA which is several times the targeted value of plasma current at initiation phase. Thus, the error field produced by induced current should be taken into account for the optimization of plasma initiation analysis.

4. Voltage Optimization Procedure

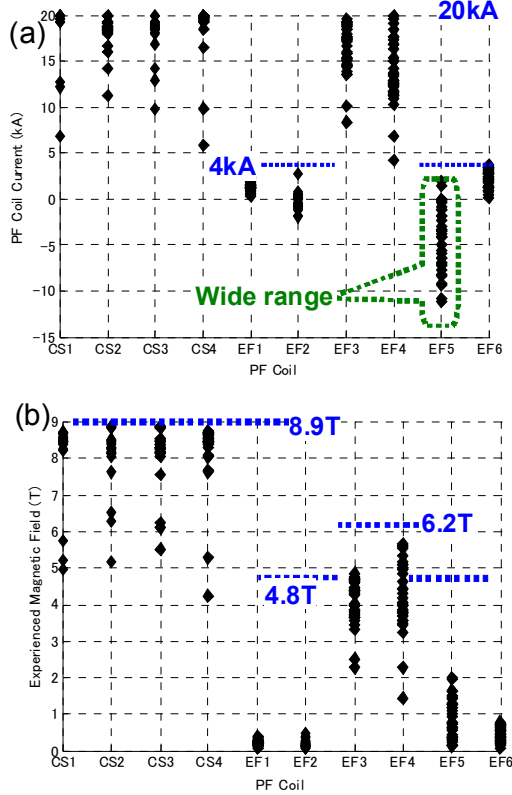


Fig. 3. Operational space of PF coil from the current and maximum experienced field strength. (a) coil current. (b) maximum experienced field strength.

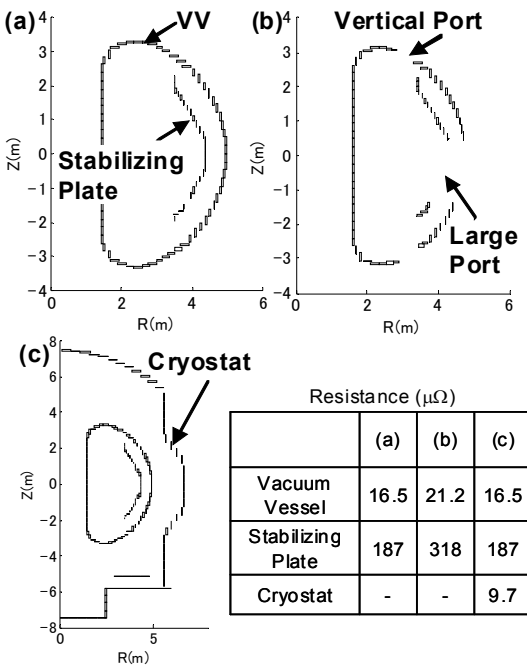


Fig. 4. Passive structure model. (a) closed VV&SP. (b) with large port. (c) with cryostat.

The targeted parameters of magnetic field for stable breakdown can be summarized as follows:

- (1) Breakdown electric field: 0.5 V/m ,
- (2) Error field: area $> 1 \text{ m}^2$ with $B_{\text{err}} < 1 \text{ mT}$,
- (3) Supplied flux: $\Psi_{\text{BD}} \sim 18 \text{ Wb}$,

In general, the connection length (C-L) is the most important parameter, but it is here taken into account in (1) and (2). On the contrary, the constraining conditions are provided as follows:

- (a) Maximum coil current: $I_{\text{max}} < 20 \text{ kA}$,
- (b) Maximum magnetic field at CS: $B_{\text{max}} < 8.9 \text{ T}$,
- (c) Maximum applied voltage: $V_{\text{PF}} < 5 \text{ kV}$,

Here, it must be noted that the available voltage of each PF coil has limitation on the control flexibility coming from the power supply configuration. The CS1-4 and EF3-4 (divertor coils) have Switching Network Unit (SNU) as a high voltage generation circuit which consists of DC current interrupter and resistor. Then the SNU does not have voltage control capability. While, Booster Thyristor Converter for the outer equilibrium field coils (EF1-2, EF5-6) can produce any demanded voltage in the range of operational limit[6].

It is clear that larger number of freedom degree has advantage for fine tuning of the objective parameters mentioned above, but simpler solution is preferable in the actual operation. Figure 5 shows some possible voltage pattern of PF coil to be applied at plasma breakdown.

Type 1 is the simplest case, because the voltage is assumed to be zero-order hold for each control cycle. This has merit of simplicity in power supply control. However, very rapid voltage control like as step function is required. Type 2 has one-order hold waveform [7]. Even in the case of single control cycle, the number of freedom degree can be raised twice in comparison to Type 1. Type 3 is similar to Type 2 except for continuity of the voltage waveform. This

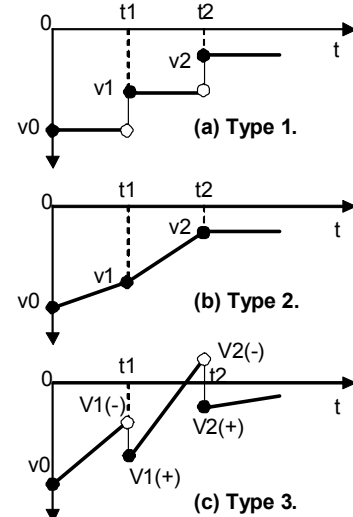


Fig. 5. Voltage pattern of PF coil to be applied.

type also requires fast voltage change similarly to Type 1.

In all cases, the experienced magnetic field \mathbf{B}_{\max} at conductor surface can be expressed by

$$[\mathbf{B}_{\max}] = [\mathbf{C}_1] [\mathbf{I}_0], \quad (1)$$

where, $[\mathbf{I}_0]$ is a PF coil current vector at $t = 0$, and $[\mathbf{C}_1]$ is a coefficient matrix.

In the case of Type 1 algorithm with 2 control cycle, the magnetic performance at reference points can be given by

$$[\Psi, d\Psi/dt, \mathbf{B}_R, \mathbf{B}_Z, dB_Z/dt]^T = [\mathbf{C}_2] [\mathbf{I}_0, \mathbf{V}_0, \mathbf{V}_1]^T, \quad (2)$$

here, $d\mathbf{B}_Z/dt$ is the derivative of vertical field and it must be compatible with dI_p/dt defined by breakdown electric field $d\Psi/dt$ and self inductance of initial plasma. \mathbf{V}_0 and \mathbf{V}_1 are PF coil voltage vector at $t=0$, and t_1 .

In the case of Type 2 and 3, the right hand variables shall be rewritten to increase the degree of freedom like as $[\mathbf{I}_0, \mathbf{V}_0, \mathbf{V}_1, \mathbf{V}_2]^T$ for Type 2 or $[\mathbf{I}_0, \mathbf{V}_0, \mathbf{V}_{1(-)}, \mathbf{V}_{1(+)}, \mathbf{V}_{2(-)}]^T$ for type 3. The optimization process will be done by iteration using the proper weight function w_i to take into account the constraining conditions.

$$\mathbf{E} = f\{\mathbf{w}_1 \cdot \mathbf{B}_{\max}, \mathbf{w}_2 \cdot \Psi, \mathbf{w}_3 \cdot d\Psi/dt, \mathbf{w}_4 \cdot \mathbf{B}_R, \mathbf{w}_5 \cdot \mathbf{B}_Z, \mathbf{w}_6 \cdot dB_Z/dt\} \quad (3)$$

Actually, each algorithm has both merit and demerit, because it strongly depends on the performance of power

Table 3. SNU resistors.

Item	Resistance (Ω)	Current (kA)	Dump Energy (MJ)
R14	3.75	1.33	2
R13	1.88	2.67	4
R12	0.94	5.33	8
R11	0.47	10.67	16
R21/R22	0.05	10	30

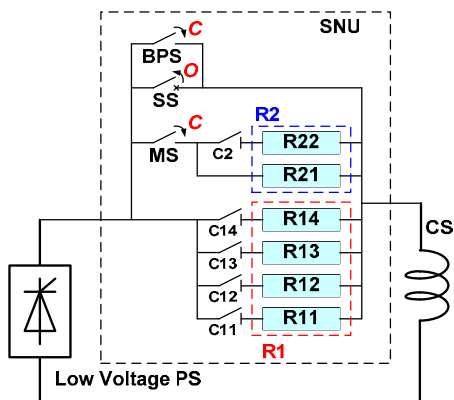


Fig. 6. Simplified circuit of Switching Network Unit (SNU) for CS circuit.

supply. Here, we have studied carefully mainly on Type 1

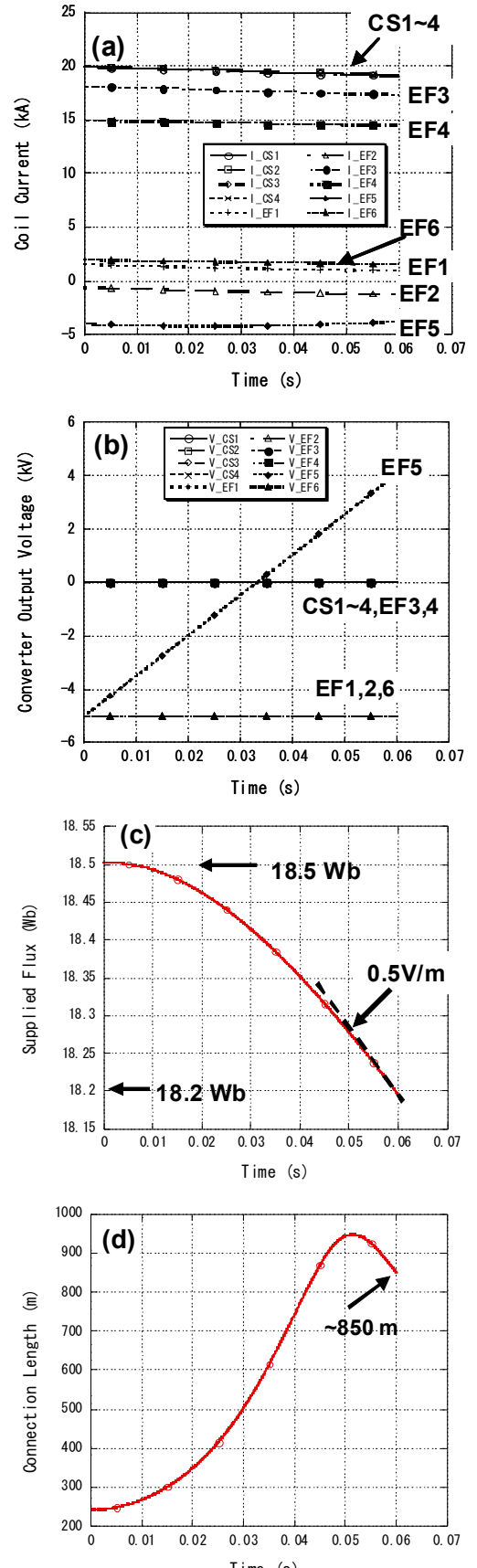


Fig. 7. Calculation result from full pre-magnetization.

and 2 methods, and confirmed that both methods can be useful. The important point is the circuit configuration of SNU, because the coil voltage of CS1-4 and EF3-4 during the breakdown phase is defined by the pre-magnetization current and the selected resistance. In the case of JT-60SA, only four EF coils (EF1-2,5-6) have Booster Thyristor Converters for the magnetic field control.

5. Switching Network Unit

Table 3 and figure 6 show the present design of switching network (SNU) of CS in JT60SA. R1 is used mainly for plasma breakdown, while R2 is complementarily added to support plasma current ramp-up after successful breakdown. From a view point of maximizing the flexibility of SNU, a unique proposal was made for ITER [8]. However, we have adopted here the simplest design choice. The R1 consists of 15 identical modular resistors and 4 selectors. The modular resistors are connected in parallel by binary system to maximize the operational flexibility. By connecting additional resistor R2 in parallel to R1 after the successful plasma breakdown, the total resistance will decrease during a shoot. It will be used while the coil current is positive.

6. Calculation Result

Figure 7 is a typical plasma breakdown scenario from the full pre-magnetization, i.e. the maximum current of 20 kA and the magnetic field strength of 8.9 T at CS. The maximum voltage of 5 kV was applied to all PF coils at $t=0$. In this case, the optimization procedure of Type-2 was used with single control cycle time of 60 ms, considering the time constant of magnetic field penetration. Here, the presence of cryostat and ports are neglected for simplicity (Fig. 4 (a)). The maximum supplied flux of 18.2 WB at breakdown was obtained in this case. It is close to the targeted value of supplied flux to sustain 5.5 MA plasmas with flattop period of 100 s. The error field was in order of 5 mT at $t = 0$ s as shown in Fig. 8(a), but it was optimized successfully at $t = 60$ ms as shown in Fig. 8(b). Booster Converter output voltages of EF1-2 and EF6 are kept to -5 kV to produce the breakdown electric field of -0.5 V/m. Only one EF coil (EF5) was used to adjust the induced current in the passive structures as shown in Fig. 7(b). The connection length of ~ 850 m was obtained (Fig. 7 (d)).

7. Discussion

The effect of cryostat and port on the error field was evaluated. In the case of Fig. 4(c) model, a very similar result with Fig. 8 was obtained except a small difference of the magnetic penetration time into the breakdown area. On the contrary, in the case of Fig. 4(b) which has large horizontal port, the error field has increased considerably

as shown in Fig. 9. It can be considered that this difficulty comes from the top-bottom asymmetry characteristics of the passive structures. To solve or mitigate this difficulty, the targeted null field area should be shifted down. Figure 10 shows that the improved error magnetic field by shifting down of the reference area by 0.6 m as shown in Fig. 10.

Above result suggests us that too much different top-bottom asymmetry characteristics at each toroidal section may cause the serious trouble of stable plasma breakdown in JT-60SA. However, the actual top-bottom asymmetry characteristics should be mitigated rather than 2D model, because the number of large horizontal port is 7 of total 18 sections. Nevertheless, the top-bottom asymmetry must be studied further in the future, because the majority of the large tokamaks built in the world have

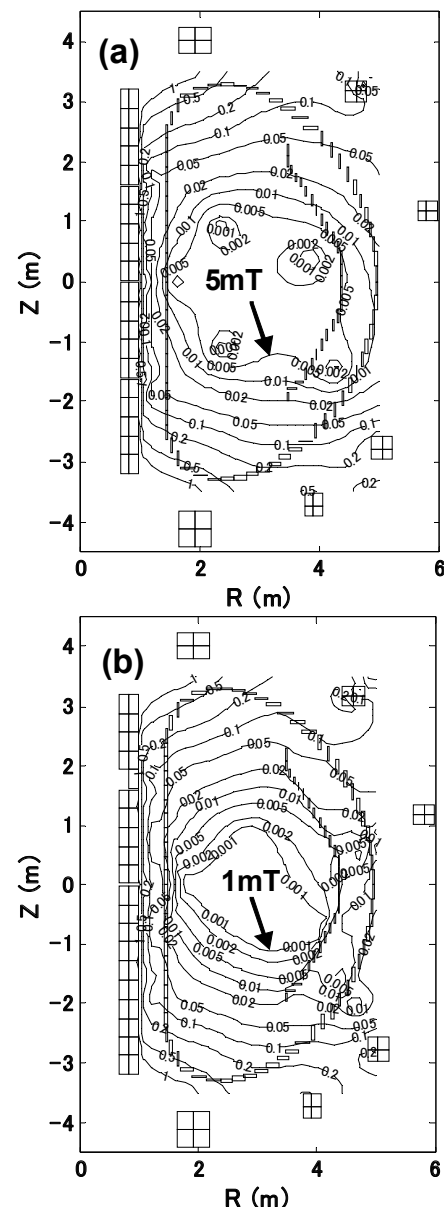
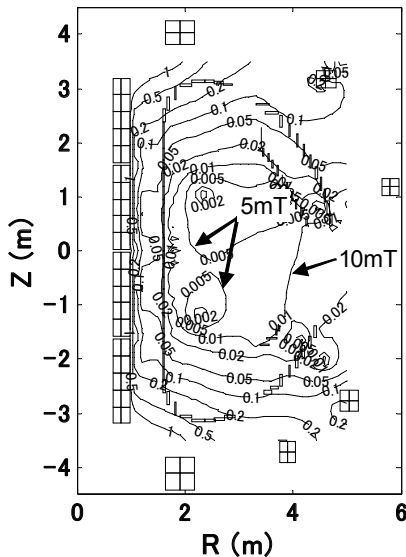
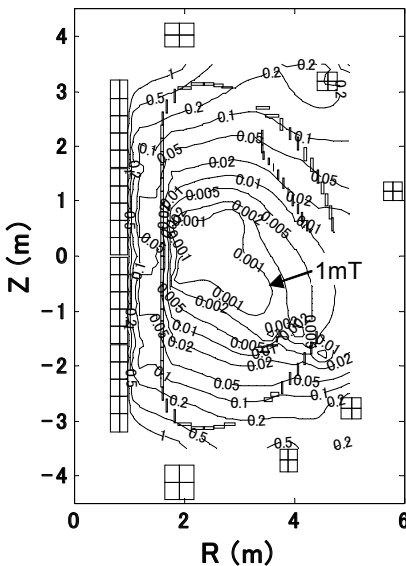


Fig. 8. Error field strength at $t=0$ (a), $t=60$ ms (b).

Fig. 9. Error field due to presence of ports at $t = 60$ ms.Fig. 10. Optimized result for port present model at $t = 60$ ms.

almost top-bottom symmetric geometry.

In the actual plasma experiments, the full pre-magnetization will not be always used, because the maximum flux swing is not necessary in many physics experiments. Table 4 shows the summary of magnetic performance in the range of 20~100% pre-magnetization. These values may change due to the available SNU resister, but satisfactory results are obtained.

8. Summary

Plasma initiation study of JT-60SA was carried out as a part of power supply system design. In conclusion, stable

plasma initiation can be expected, because the satisfactory results were obtained in 2D models. However, the top-bottom asymmetry characteristics of passive structure may cause the trouble of plasma initiation. It shall be analyzed further using more precise model.

Table 4. Obtained magnetic field performances.

$\Psi(0)$ (Wb)	C-L (m)	Electric Field (V/m)
3.40	1131	-0.49
5.29	947	-0.48
7.07	1361	-0.50
8.98	910	-0.50
10.5	1486	-0.50
12.7	1037	-0.50
14.5	962	-0.50
16.4	896	-0.50
18.2	850	-0.50

Notice: $\Psi(0)$ is the supplied flux at $t = 60$ ms.

C-L means connection length.

Electric Field is defined at $R=2.8$ m.

Acknowledgement

This work was supported within the framework of the "Broader Approach International Agreement". The authors would like to express their thanks to Drs. R. Piovan and I. Senda for their continuous support.

References

- [1] I Senda et al., "Simulation studies of plasma initiation and disruption in JT-60U", *Fusion Eng. and Des.* **45** (1999) 15-29.
- [2] B.J. Xiao et al., "EAST plasma control system", *Fusion Engineering and Design* **83** (2008) 181-187.
- [3] I Senda et al., "Optimization of plasma initiation in the ITER Tokamak", *Fusion Eng. and Des.* **42** (1998) 395-399.
- [4] M. Matsukawa et al., "Status of JT-60SA tokamak under the EU-JA Broader Approach Agreement", *Fusion Eng. and Des.* **83** (2008) 795-803.
- [5] C. Darbos et al., "Progress in design and integration of the ITER Electron Cyclotron H&D System", *Fusion Eng. and Des.* **84** (2009) 651-655.
- [6] K. Shimada et al., "A Design Study of Stable Coil Current Control Method for Back-to-Back Thyristor Converter in JT-60SA", this conference.
- [7] I. Senda, T. Shoji, S. Nishio et al., "Optimizing voltage waveforms of poloidal field coils at the plasma breakdown", JAERI-Tech 96-016, 1996.
- [8] B. Bareyt and S. Bulgakov, "A New optimized design concept of the switching network resistors of the large ITER-FEAT tokamak", *Fusion Eng. and Des.* **60** (2002) 127-140.